Clim. Past, 10, 251–260, 2014
www.clim-past.net/10/251/2014/
doi:10.5194/cp-10-251-2014

Climate of the Past
Open Access

Salinity changes in the Agulhas leakage area recorded by stable hydrogen isotopes of C_{37} alkenones during Termination I and II

S. Kasper[1], M. T. J. van der Meer[1], A. Mets[1], R. Zahn[2,3], J. S. Sinninghe Damsté[1], and S. Schouten[1]

[1]NIOZ Royal Netherlands Institute for Sea Research, Department of Marine Organic Biogeochemistry, P.O. Box 59, 1790 AB Den Burg (Texel), the Netherlands
[2]Institució Catalana de Recerca i Estudis Avançats, ICREA, Barcelona, Spain
[3]Universitat Autònoma de Barcelona, Institut de Ciència i Tecnologia Ambientals (ICTA) and Departament de Física, 08193 Bellaterra, Spain

Correspondence to: S. Kasper (sebastian.kasper@nioz.nl)

Received: 13 May 2013 – Published in Clim. Past Discuss.: 18 June 2013
Revised: 13 December 2013 – Accepted: 16 December 2013 – Published: 5 February 2014

Abstract. At the southern tip of Africa, the Agulhas Current reflects back into the Indian Ocean causing so-called "Agulhas rings" to spin off and release relatively warm and saline water into the South Atlantic Ocean. Previous reconstructions of the dynamics of the Agulhas Current, based on paleo-sea surface temperature and sea surface salinity proxies, inferred that Agulhas leakage from the Indian Ocean to the South Atlantic was reduced during glacial stages as a consequence of shifted wind fields and a northwards migration of the subtropical front. Subsequently, this might have led to a buildup of warm saline water in the southern Indian Ocean. To investigate this latter hypothesis, we reconstructed sea surface salinity changes using alkenone δD, and paleo-sea surface temperature using TEX_{86}^{H} and $U_{37}^{K'}$, from two sediment cores (MD02-2594, MD96-2080) located in the Agulhas leakage area during Termination I and II. Both $U_{37}^{K'}$ and TEX_{86}^{H} temperature reconstructions indicate an abrupt warming during the glacial terminations, while a shift to more negative $\delta D_{alkenone}$ values of approximately 14 ‰ during glacial Termination I and II is also observed. Approximately half of the isotopic shift can be attributed to the change in global ice volume, while the residual isotopic shift is attributed to changes in salinity, suggesting relatively high salinities at the core sites during glacials, with subsequent freshening during glacial terminations. Approximate estimations suggest that $\delta D_{alkenone}$ represents a salinity change of ca. 1.7–1.9 during Termination I and Termination II. These estimations are in good agreement with the proposed changes in salinity derived from previously reported combined planktonic Foraminifera $\delta^{18}O$ values and Mg/Ca-based temperature reconstructions. Our results confirm that the δD of alkenones is a potentially suitable tool to reconstruct salinity changes independent of planktonic Foraminifera $\delta^{18}O$.

1 Introduction

Approximately 2–15 Sv of warm and saline Indian Ocean water is annually released into the South Atlantic Ocean by the Agulhas Current, an ocean current system that is confined by the subtropical front (STF) and the southern African coast (Lutjeharms, 2006). The Agulhas Current is fed by warm, saline Indian Ocean water from two sources: the Mozambique Channel, between Madagascar and the East African coast, and the East Madagascar Current, which merges with the Mozambique Channel flow at approximately 28° S (Penven et al., 2006). When this warm, saline water reaches the Agulhas corridor at the tip of Africa, the vast majority is transported back into the Indian Ocean via the Agulhas return current (Fig. 1). However, between five and seven rings of warm, saline water are released into the Atlantic Ocean per year, termed Agulhas leakage (Lutjeharms, 2006). These Agulhas rings of Indian Ocean waters have been shown to play an important role in the heat and salt budget in the Atlantic Ocean, thereby impacting the Atlantic Meridional Overturning Circulation (AMOC) (Peeters et al., 2004; Biastoch et al., 2008; Bard and Rickaby, 2009; Haarsma et al., 2011; van Sebille et al., 2011).

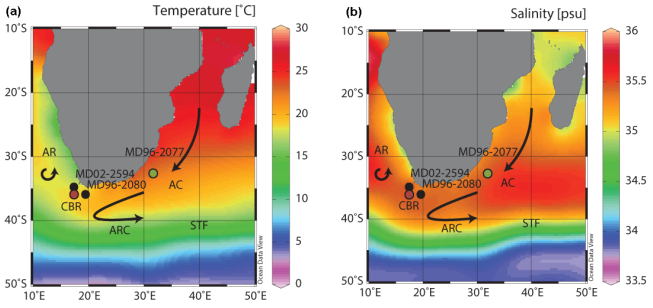

Fig. 1. Location of the cores MD02-2594 and MD96-2080 (black dots) and reference site Cape Basin record (CBR, red dot) (Peeters et al., 2004), MD96-2077 (green dot) (Bard and Rickaby, 2009) and oceanographic setting on **(a)** a map of modern sea surface temperatures and **(b)** a map of modern sea surface salinity. Agulhas Current (AC), Agulhas return current (ARC), Agulhas rings (AR) and subtropical front (STF). The underlying maps of modern sea surface temperatures and salinity were compiled with high-resolution CTD data from http://www.nodc.noaa.gov and the Ocean Data View software version 4.3.7 by Schlitzer, R., Ocean Data View (http://odv.awi.de), 2010.

The magnitude of Agulhas leakage into the Atlantic Ocean depends on the strength of the Agulhas Current as well as the position of the retroflection (Lutjeharms, 2006). However, the effect of Agulhas Current strength on the Agulhas leakage efficiency is still debated. For instance, Rouault et al. (2009) suggested that, based on recent temperature observations and modeling experiments, increased Agulhas leakage of warm and saline waters into the South Atlantic Ocean can be associated with increased Agulhas Current transport, while modeling experiments performed by van Sebille et al. (2009) suggested increased Agulhas leakage to be associated with a weakened Agulhas Current.

Previous studies have shown that during glacial stages a weakened and more variable Agulhas Current occurs together with reduced Agulhas leakage (Peeters et al., 2004; Franzese et al., 2006). Peeters et al. (2004) found relatively low contributions of "Agulhas leakage fauna" in the Cape Basin, suggesting a reduced Agulhas leakage during glacial stages (Rau et al., 2002; Peeters et al., 2004), coinciding with low sea surface temperatures (SSTs). This suggests a restriction in the Agulhas leakage during cold periods (Peeters et al., 2004). Furthermore, deep-ocean stable carbon isotope gradients have been applied in combination with sea surface temperature reconstructions as indicators of a connection between deep-water ventilation and Agulhas leakage strength (Bard and Rickaby, 2009). The results demonstrate that a reduced leakage typically correlates with reduced deep ventilation (Bard and Rickaby, 2009).

A northward shift of the STF and eastward forcing of the retroflection during glacial periods may have led to an increased back transport of warm, saline water into the Indian Ocean during glacial periods (Peeters et al., 2004). Martinez-Mendez et al. (2010) showed increased sea water oxygen isotope ($\delta^{18}O_{sw}$) values, derived from paired planktonic Foraminifera $\delta^{18}O$ and Mg/Ca analysis of *Globigerina bulloides*, in the Agulhas leakage area throughout marine isotope stage 6 (MIS6) and marine isotope stage 3 (MIS3) and early marine isotope stage 2 (MIS2). These elevated $\delta^{18}O_{sw}$ values are likely indicative for increased salinity (Martinez-Mendez et al., 2010). However, it should be noted that salinity reconstructions, based on planktonic Foraminifera $\delta^{18}O_{sw}$ values, carry some uncertainties that are difficult to constrain, e.g., assumed constancy for the transfer functions of $\delta^{18}O_{sw}$ to salinity over space and time (Rohling and Bigg, 1998; Rohling, 2000).

Martinez-Mendez et al. (2010) further reported that reconstructed SST, derived from the planktonic Foraminifera Mg/Ca of *G. bulloides*, displayed a gradual warming trend starting in the early MIS6 and MIS2 (Martinez-Mendez et al., 2010). This is, however, in contradiction with temperature reconstructions based on $U^{K'}_{37}$ paleothermometry (Peeters et al., 2004; Martinez-Mendez et al., 2010), which showed cooler sea surface temperatures during glacial periods, followed by a rapid warming at the onset of the interglacial stages. These differences may be related to uncertainties associated with the different temperature proxies (Bard, 2001). Planktonic foraminiferal Mg/Ca ratios have been shown to reflect not only temperature, but also salinity (Ferguson et al., 2008; Arbuszewski et al., 2010, Hönisch et al., 2013). This has been demonstrated in high-salinity environments such as the Mediterranean Sea (Ferguson et al., 2008), and in open ocean settings such as the tropical Atlantic Ocean (Arbuszewski et al., 2010). Furthermore, $U^{K'}_{37}$–SST relationships are derived from photosynthetic haptophyte algae with different growth seasons and (depth) habitats than the planktonic Foraminifera *G. bulloides*, potentially recording different temperature ranges (Prahl and Wakeham, 1987; Bard, 2001).

We use the hydrogen isotope composition of the combined $C_{37:2-3}$ alkenones ($\delta D_{alkenone}$), produced by haptophyte algae, as a proxy for relative changes in sea surface salinity (SSS). Culture experiments for two common open ocean haptophyte species – *Emiliania huxleyi* and *Gephyrocapsa oceanica* – have shown that the hydrogen isotope composition of alkenones is mainly dependent on salinity, the hydrogen isotope composition of the growth media and, to a lesser extent, growth rate (Englebrecht and Sachs, 2005; Schouten et al., 2006). Furthermore, van der Meer et al. (2013) showed that measuring the combined $C_{37:2-3}$ $\delta D_{alkenone}$ rather than separated $C_{37:2}$ and $C_{37:3}$ alkenones yields a more robust water δD and salinity signal, possibly by reducing biosynthetic effects related to the synthesis of the $C_{37:3}$ alkenones from the $C_{37:2}$ (Rontani et al., 2006). Application of the hydrogen isotope composition of alkenones has resulted in reasonable salinity reconstructions for the eastern Mediterranean and Black Sea (van der Meer et al., 2007, 2008) and hydrological reconstructions in the Panama Basin (Pahnke et

al., 2007). Here, we apply the $\delta D_{alkenone}$ to estimate relative salinities of the Agulhas system focusing on Termination I and Termination II using the same cores used by Martinez-Mendez et al. (2010), situated in the Agulhas leakage area, off the coast of South Africa (Fig. 1). In order to assess the effect of growth rates on $\delta D_{alkenone}$, we measure the stable carbon isotope composition of the combined $C_{37:2-3}$ alkenones ($\delta^{13}C_{alkenones}$) on samples from glacials and interglacials (Rau et al., 1996; Bidigare et al., 1997; Schouten et al., 2006). Furthermore, we reconstruct SST using the TEX_{86}^{H} proxy (Schouten et al., 2002; Kim et al., 2010) and compare this with the $U_{37}^{K'}$ and Mg/Ca record of the planktonic Foraminifera *G. bulloides* for the same sediment cores (Martinez-Mendez et al., 2010).

1.1 Material and methods

Sediment samples were taken from cores MD96-2080 (36°19.2′ S, 19°28.2′ E; 2488 m water depth) and MD02-2594 (34°42.6′ S, 17°20.3′ E; 2440 m water depth) from the Agulhas bank slope off the coast of southern South Africa (Fig. 1). Core MD02-2594 was taken during the RV *Marion Dufresne* cruise MD128 SWAF (Giraudeau et al., 2003). Core MD96-2080 was obtained during the IMAGES II Campaign NAUSICAA (Bertrand, 1997). Age models and records of *Globigerina bulloides* $\delta^{18}O$ and Mg/Ca have previously been established for both sediment cores (Martinez-Mendez et al., 2008, 2010). The sampled interval of core MD02-2594 covered the period 3 to 42 ka (MIS1 to mid-MIS3) and included Termination I. Core MD96-2080 covered the period between 117 and 182 ka (MIS5e to MIS6) and included Termination II (Tables 1, 2).

1.2 Sample preparation

Sediment samples were freeze-dried and homogenized with a mortar and pestle. The homogenized material was then extracted using the accelerated solvent extractor method (ASE) with dichloromethane (DCM) : methanol 9 : 1 (v / v) and a pressure of 1000 psi in three extraction cycles. The total lipid extract was separated over an Al_2O_3 column into a apolar, ketone and polar fraction using hexane : DCM 9 : 1, hexane : DCM 1 : 1 and DCM : methanol 1 : 1, respectively. The ketone fraction was analyzed for $U_{37}^{K'}$ using gas chromatography. Gas chromatography/high-temperature conversion/isotope ratio mass spectrometry (GC/TC/irMS) was used to measure the combined hydrogen isotope composition of the di- and tri-unsaturated C_{37} alkenones. The polar fraction was analyzed for TEX_{86}^{H} using high-performance liquid chromatography mass spectrometry (HPLC/MS). Stable carbon isotopes of the combined di- and tri-unsaturated C_{37} alkenones were analyzed using GC/combustion/irMS.

Table 1. Results for combined $C_{37:2-3}$alkenone stable hydrogen isotope ($\delta D_{alkenone}$, ‰), stable carbon isotope ($\delta^{13}C_{alkenone}$, ‰), TEX_{86}^{H} SST and $U_{37}^{K'}$ SST analyses for core MD96-2080.

Age (ka)	$U_{37}^{K'}$	TEX_{86}^{H}	$\delta D_{alkenone}$ (‰)[a]	$\delta^{13}C_{alkenone}$ (‰)[a]
117.7	0.819	−0.276	−197 ± 2	
119.9	0.819	−0.272	−196 ± 2	
123.1	0.856	−0.277	−180	
125.4	0.864	−0.278	−193 ± 4	−24.7 ± 0.5
126.5	0.833	−0.273	−194 ± 1	−25.4 ± 0.2
127.0	0.829	−0.274	−198 ± 0	
127.9	0.845	−0.275	−188 ± 1	−25.1 ± 0.8
128.7	0.851	−0.266	−194 ± 4	−25.6 ± 0.4
129.8	0.828	−0.248	−194 ± 0	
131.3	0.821	−0.253	−192 ± 3	
132.8	0.798	−0.250	−189 ± 2	−24.2 ± 0.4
133.6	0.819	−0.238	−190 ± 0	−23.9 ± 0.1
135.1	0.776	−0.235	−182 ± 2	
137.3	0.750	−0.251	−182 ± 4	−24.5 ± 0.1
137.7	0.749	−0.256	−183 ± 1	−24.1 ± 0.4
141.2	0.709	−0.321	−179 ± 1	
142.2	0.710	−0.320	−177 ± 3	
145.0	0.717	−0.325	−180 ± 1	−24.9 ± 0.1
147.5	0.726	−0.309		
151.5	0.707	−0.314	−184 ± 2	−24.8 ± 0.6
152.0	0.734	−0.314	−182 ± 0	
154.7	0.724	−0.330	−186 ± 1	−24.6 ± 0.2
158.0	0.738	−0.290	−177 ± 0	
162.3	0.745	−0.332	−179 ± 3	
168.8	0.745	−0.314	−191 ± 2	
177.9	0.714	−0.292	−190 ± 3	
182.7	0.707	−0.303	−187 ± 3	

[a] The error is defined as the range of duplicated measurements.

1.3 $U_{37}^{K'}$ analysis

Ketone fractions were analyzed by gas chromatography (GC) using an Agilent 6890 gas chromatograph with a flame ionization detector and a Agilent CP Sil-5 fused silica capillary column (50 m × 0.32 mm, film thickness = 0.12 µm) with helium as the carrier gas. The GC oven was programmed to increase the temperature subsequently from 70 to 130 °C at 20 °C min^{-1} , and then at 4 °C min^{-1} to 320 °C, at which it was held isothermal for 10 min. $U_{37}^{K'}$ values were calculated according to Prahl and Wakeham (1987). Subsequently, SST was calculated using the core top calibration established by Müller et al. (1998).

1.4 δD of alkenone analysis

Alkenone hydrogen isotope analyses were carried out on a Thermo Finnigan DELTA^{Plus} XL GC/TC/irMS. The temperature conditions of the GC increased from 70 to 145 °C at 20 °C min^{-1}, then to 320 °C at 4 °C min^{-1}, at which it was held isothermal for 13 min using an Agilent CP Sil-5

Table 2. Results for combined $C_{37:2-3}$ alkenone stable hydrogen isotope ($\delta D_{alkenone}$, ‰), stable carbon isotope ($\delta^{13}C_{alkenone}$, ‰) TEX_{86}^{H} SST and $U_{37}^{K'}$ SST analyses for core MD02-2594.

Age (ka)	$U_{37}^{K'}$	TEX_{86}^{H}	δD alkenone (‰)[a]	δ^{13}C alkenone (‰)[a]
3.5	0.724	−0.305	−192 ± 2	−24.1 ± 0.1
5.6	0.723	−0.307	−184 ± 2	
6.3	0.746	−0.309	−189 ± 4	
6.9	0.736	−0.311	−182 ± 1	
8.6	0.753	−0.308	−191 ± 3	
12.0	0.762	−0.282	−178 ± 2	−24.1 ± 0.8
18.0	0.685	−0.308	−179 ± 1	
18.5	0.677	−0.366	−171 ± 2	
21.1	0.672	−0.336	−173 ± 3	−24.2 ± 1.1
22.3	0.686	−0.352	−178 ± 2	
26.7	0.686	−0.328	−166 ± 2	
28.4	0.682	−0.333	−173 ± 0	
29.5	0.686	−0.339	−172 ± 1	
30.8	0.715	−0.313	−179 ± 2	
31.5	0.692	−0.332	−173 ± 2	−23.6 ± 0.1
32.0	0.696	−0.315	−177 ± 1	
37.4	0.728	−0.312	−171 ± 3	
42.1	0.676	−0.343	−180 ± 2	

[a] The error is defined as the range of duplicated measurements.

column (25 m × 0.32 mm) with a film thickness of 0.4 µm and 1 mL min^{-1} helium at constant flow. The thermal conversion temperature was set to 1425 °C. The H_3^+ correction factor was determined daily and ranged between 10 and 14. Isotopic values for alkenones were standardized against pulses of H_2 reference gas, which was injected three times at the beginning and two times at the end of each run. A set of standard *n*-alkanes with known isotopic composition (Mixture B prepared by Arndt Schimmelmann, University of Indiana) was analyzed daily prior to each sample batch in order to monitor the system performance. Samples were only analyzed when the alkanes in Mix B had an average deviation from their off-line determined value of < 5 ‰. Squalane was co-injected as an internal standard with each sample to monitor the precision of the alkenone isotope values. The squalane standard yielded an average δD value of −167 ‰ ± 4.5, which compared favorably with its offline determined δD value of −170 ‰. Alkenone δD values were measured as the combined peak of the $C_{37:2}$ and $C_{37:3}$ alkenones (van der Meer et al., 2013), and fractions were analyzed in duplicates if a sufficient amount of sample material was available. Standard deviations of replicate analyses varied from ±0.1 ‰ to ±5.9 ‰.

1.5 δ^{13}C of alkenone analyses

Combined $C_{37:2-3}$ alkenones were analyzed using a Thermo Delta V isotope ratio monitoring mass spectrometer coupled to an Agilent 6890 GC. Samples were dissolved in hexane and analyzed using a GC temperature program starting at 70 °C, then increasing to 130 °C at 20 °C min^{-1}, and then to 320 °C at 4 °C min^{-1}, where it was held for 20 min. The stable carbon isotope compositions for $\delta^{13}C_{alkenone}$ are reported relative to Vienna Pee Dee Belemnite (VDPB). The $\delta^{13}C_{alkenone}$ values are averages of at least two runs. GC-irMS performance was checked daily by analyzing a standard mixture of *n*-alkanes and fatty acids, including two fully perdeuterated alkanes with a known isotopic composition. These perdeuterated alkanes were also co-injected with every sample analysis and yielded an average δ^{13}C value of −32.5 ± 0.5 ‰ and −27.0 ± 0.5 ‰ for *n*-C_{20} and *n*-C_{24}, respectively. This compared favorably with their offline determined δ^{13}C values of −32.7 ‰ and −27.0 ‰ for *n*-C_{20} and *n*-C_{24}, respectively.

1.6 TEX_{86}^{H} analysis

Analyses for TEX_{86}^{H} were performed as described by Schouten et al. (2007). In summary, an Agilent 1100 series HPLC/MS equipped with an auto-injector and Agilent ChemStation chromatography manager software was used. Separation was achieved on an Alltech Prevail Cyano column (2.1 × 150 mm, 3 µm), maintained at 30 °C. Glycerol dibiphytanyl glycerol tetraethers (GDGTs) were eluted with 99 % hexane and 1% propanol for 5 min, followed by a linear gradient to 1.8 % propanol in 45 min, followed by backflushing hexane/propanol (9 : 1, v / v) at 0.2 mL min^{-1} for 10 min. Detection was achieved using atmospheric pressure positive ion chemical ionization mass spectrometry (APCI-MS) of the eluent. Conditions for the Agilent 1100 APCI-MS were as follows: nebulizer pressure of 60 psi, vaporizer temperature of 400 °C, drying gas (N_2) flow of 6 L min^{-1} and temperature 200 °C, capillary voltage of −3 kV and a corona of 5 µA (∼ 3.2 kV). GDGTs were detected by single ion monitoring (SIM) of their $[M+H]^+$ ions (dwell time = 234 ms) (Schouten et al., 2007) and quantified by integration of the peak areas. The TEX_{86}^{H} values and absolute temperatures were calculated according to Kim et al. (2010). This calibration is recommended for temperature reconstruction above 15 °C (Kim et al., 2010) and therefore appears to be the most suitable model for reconstructing subtropical temperatures, as found in the Agulhas leakage area.

2 Results

2.1 Sea surface temperature proxies

The $U_{37}^{K'}$ record of MD96-2080 indicated constant temperatures of approximately 20.7 ± 0.5 °C throughout MIS6 (138–182 ka) (Table 1, Fig. 2). With the onset of Termination II at approximately 138 ka, temperatures began to increase to a maximum of ∼ 25 °C during early MIS5e (∼ 125 ka), followed by a slight decrease in temperature towards ∼ 23 °C at about 120 ka. The $U_{37}^{K'}$ SST record for MD02-2594 indicated

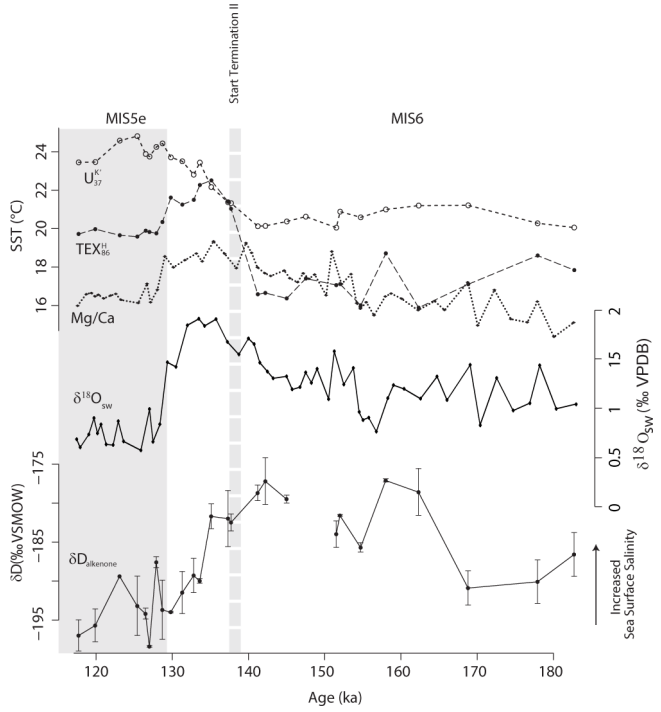

Fig. 2. Reconstructed SST of $U^{K'}_{37}$ (dashed line, open circles), TEX^{H}_{86} (dashed line, closed circles), Mg/Ca of *G. bulloides* (dotted line, closed circles, Martinez-Mendez et al., 2010), reconstructed $\delta^{18}O_{sw}$ from *G. bulloides* (solid line, diamonds, Martinez-Mendez et al., 2010) and hydrogen isotope composition of $C_{37:2-3}$ alkenones (solid line, closed circles) for core MD96-2080.

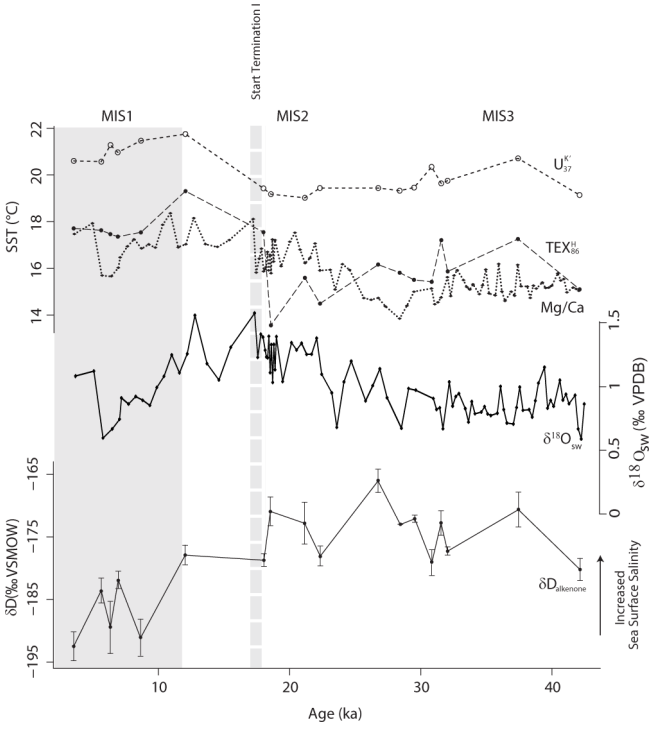

Fig. 3. Reconstructed SST of $U^{K'}_{37}$ (dashed line, open circles), TEX^{H}_{86} (dashed line, closed circles), Mg/Ca of *G. bulloides* (dotted line, closed circles, Martinez-Mendez et al., 2010), reconstructed $\delta^{18}O_{sw}$ from *G. bulloides* (solid line, diamonds, Martinez-Mendez et al., 2010) and hydrogen isotope composition of $C_{37:2-3}$ alkenones (solid line, closed circles) for core MD02-2594.

relatively constant temperatures of 20 ± 0.5 °C throughout MIS3 and early MIS2 (Table 2, Fig. 3). With the onset of Termination I during mid-MIS2 ($\sim$ 18 ka), temperatures showed a slight warming towards $\sim$ 22 °C at the beginning of MIS1. Throughout MIS1, temperatures slightly decreased to approximately 21 °C.

The overall pattern in the TEX^{H}_{86} records for the two cores indicated that absolute temperatures were cooler by up to 5 °C compared to $U^{K'}_{37}$ temperatures during glacial and interglacial stages MIS5e and MIS6, as well as MIS3/MIS2 and MIS1. During MIS6, TEX^{H}_{86} temperatures were relatively stable at 17 ± 1 °C, although less stable than $U^{K'}_{37}$ SST (Table 1, Fig. 2). At the initial termination of the glacial MIS6 (ca. 135–138 ka), reconstructed TEX^{H}_{86} temperatures increased rapidly to about 22 °C, which is similar in absolute terms compared to $U^{K'}_{37}$ SST (Fig. 2). Subsequently, TEX^{H}_{86} SST decreased rapidly to $\sim$ 20 °C and remained constant during MIS5e. During MIS3 and early MIS2, TEX^{H}_{86} SST showed a trend towards cooler temperatures from approximately 17 °C at $\sim$ 38 ka to 14 °C at the start of Termination I (18 ka) (Table 2, Fig. 3). At the onset of Termination I, TEX^{H}_{86} SSTs abruptly increased. Temperatures reached a maximum of 19 °C at the beginning of MIS1 (11 ka) and decreased again to relatively constant temperatures of ca. 18 °C throughout MIS1. This trend is comparable to the $U^{K'}_{37}$ SST record, albeit with a negative offset of approximately 4 °C throughout MIS3/MIS2 and MIS1, and approximately 2 °C during the glacial termination phase (11–18 ka) (Fig. 3).

2.2 Stable hydrogen and carbon isotope composition of $C_{37:2-3}$ alkenones

The $\delta D_{alkenone}$ values in core MD96-2080 ranged between −177 and −198 ‰ (Table 1). During early MIS6 (169 to 181 ka), $\delta D_{alkenone}$ values were approximately -189 ± 2 ‰ and shifted to more positive values of ca. −177 ‰ at 158 ka. In the time interval between 142 and 162 ka (MIS6), $\delta D_{alkenone}$ decreased to -180 ± 3 ‰. During glacial Termination II (130 to 138 ka), the $\delta D_{alkenone}$ values decreased abruptly to approximately -194 ± 3 ‰ for MIS5e (118–130 ka) (Fig. 2). The $\delta D_{alkenone}$ values in core MD02-2594 ranged between −166 and −192 ‰ (Table 2). In the time interval from 12 to 41 ka (MIS3 and MIS2), values for $\delta D_{alkenone}$ were relatively constant at approximately -174 ± 4 ‰ (Fig. 3). At ca. 11 ka (onset of MIS1), $\delta D_{alkenone}$ values shifted to more negative values with an average of −188 ±5 ‰ for the time period of 3 to 9 ka (MIS1) (Fig. 3).

3 Discussion

3.1 Development of sea surface temperatures during Termination I and Termination II

Application of the $U^{K'}_{37}$ proxy resulted in higher reconstructed temperatures compared to the TEX^{H}_{86} and Mg/Ca SST reconstructions (Figs. 2, 3). Difference in absolute temperatures may be explained by a variety of reasons such as growth seasons and/or depth habitats between the alkenone producers, the Thaumarchaeota (GDGT producers) and the planktonic Foraminifera (Müller et al., 1998; Bard, 2001; Karner et al., 2001; Wuchter et al., 2006; Lee et al., 2008; Saher et al., 2009; dos Santos et al., 2010; Fallett et al., 2011; Huguet et al., 2011).

Both $U^{K'}_{37}$ and TEX^{H}_{86} temperatures suggest cooler conditions throughout stages MIS6 and MIS3/2 (Figs. 2, 3). This is followed by an abrupt warming during succeeding glacial terminations, leading to warmer conditions in the interglacial stages MIS5e and MIS1. The pattern fits well with $U^{K'}_{37}$-derived temperature reconstructions from other sediment cores in the area of this study site (Fig. 4) (Schneider et al., 1995; Peeters et al., 2004; Bard and Rickaby, 2009). Temperature reconstructions based on Mg/Ca and TEX^{H}_{86} show that maximum temperatures occurred during the deglaciations. However, $U^{K'}_{37}$ temperature reconstructions showed that the SST maximum occurred approximately 5 ka later than in Mg/Ca- and TEX^{H}_{86}-based reconstructions. This temperature increase could possibly point towards an increased influence of warm Indian Ocean waters, and hence increased Agulhas leakage. This increased leakage in turn is likely related to a southward shift of the subtropical front due to shifting wind fields and a southward migration of the land ice shields (Peeters et al., 2004). Nevertheless, these observations do not necessarily imply a buildup of warm Indian Ocean waters prior to glacial terminations at the core site.

Strikingly, the timing of the beginning of the warming trend reflected in the Foraminifera Mg/Ca record of *G. bulloides* (Martinez-Mendez et al., 2010) is different from the $U^{K'}_{37}$ and TEX^{H}_{86} records, as well as other $U^{K'}_{37}$ records in the region (Fig. 4) (Peeters et al., 2004).The Mg/Ca SST record identifies a warming trend starting in the early glacial periods and gradually extending over the glacial termination phases (Martinez-Mendez et al., 2010). Furthermore, a recent study by Marino et al. (2013) also showed a discrepancy between Mg/Ca of the planktonic Foraminifera *Globigerinoides ruber* and $U^{K'}_{37}$ SST. It has been reported that changes in salinity can also affect the Mg/Ca ratios in Foraminifera shells, specifically during glacial periods when salinity was likely elevated (Ferguson et al., 2008; Arbuszewski et al., 2010). Thus, the observed trends in foraminiferal Mg/Ca may result from a combined salinity and temperature signal (Hönisch et al., 2013).

3.2 Salinity changes during Termination I and Termination II

The $C_{37:2-3}$ alkenone hydrogen isotope records consistently show a substantial decrease toward more deuterium-depleted values during the glacial terminations and the interglacial stages MIS5e and MIS1 (Figs. 2, 3). We quantified changes from glacial to interglacial stages by averaging time intervals from before and after each termination. We observed average shifts in $\delta D_{alkenone}$ of approximately 14 ‰ for both Termination I and II (Table 3). These shifts in the $\delta D_{alkenone}$ values can be caused by a number of factors such as decreasing δD of sea water (δD_{sw}) as an effect of decreasing global ice volume during the terminations (Rohling, 2000), ocean salinity, algal growth rate, haptophyte species composition (Schouten et al., 2006), differences in the hydrogen isotope composition of the $C_{37:2}$ and $C_{37:3}$ alkenones (D'Andrea et al., 2007; Schwab and Sachs, 2009). However, the latter factor is likely unimportant, as for the range of $U^{K'}_{37}$ values observed in this study we expect a maximum difference of 4 ‰ in the hydrogen isotope composition between $C_{37:2}$ and $C_{37:3}$, which falls within the accuracy of the GC/TC/irMS (van der Meer et al., 2013).

In order to assess changes in growth rate for the haptophytes, we measured the stable carbon isotope composition of the combined $C_{37:2-3}$ alkenones ($\delta^{13}C_{alkenone}$) (Tables 1, 2). Our results show relatively small changes of about -0.6 ‰ and -0.3 ‰ in $\delta^{13}C_{alkenone}$ during Termination I and II, respectively. The fractionation of stable carbon isotopes is mainly controlled by physiological factors like growth rate, cell size and geometry, as well as by the supply of dissolved CO_2 (Rau et al., 1996; Bidigare et al., 1997). The more depleted alkenone $\delta^{13}C$ values during interglacials suggest either slightly higher dissolved CO_2 concentrations or lower growth rates. We suggest that higher dissolved CO_2 concentrations likely explain the more depleted alkenone $\delta^{13}C$ values as CO_2 concentrations were higher during interglacials compared to glacials (Curry and Crowley, 1987). Since reduced growth rates would result in decreasing hydrogen isotopic fractionation, our observed increase in hydrogen isotopic fractionation during interglacials compared to glacials cannot be explained by growth rate changes (Schouten et al., 2006).

Species changes could also explain the observed hydrogen isotope shift. Assemblage studies in the Agulhas leakage have shown an increasing abundance of the predominant haptophyte *E. huxleyi* from the beginning of MIS7 towards MIS1, with a maximum relative abundance observed at the onset of MIS1 (Flores et al., 1999). *G. oceanica*, however, reaches maximum relative abundances during Termination II (Flores et al., 1999). Changes in the coccolithophore assemblage toward a larger fraction of *G. oceanica* could have resulted in more negative $\delta D_{alkenone}$ values during that time since *G. oceanica* fractionates more against D than *E. huxleyi* (Schouten et al., 2006). However, the abundance of

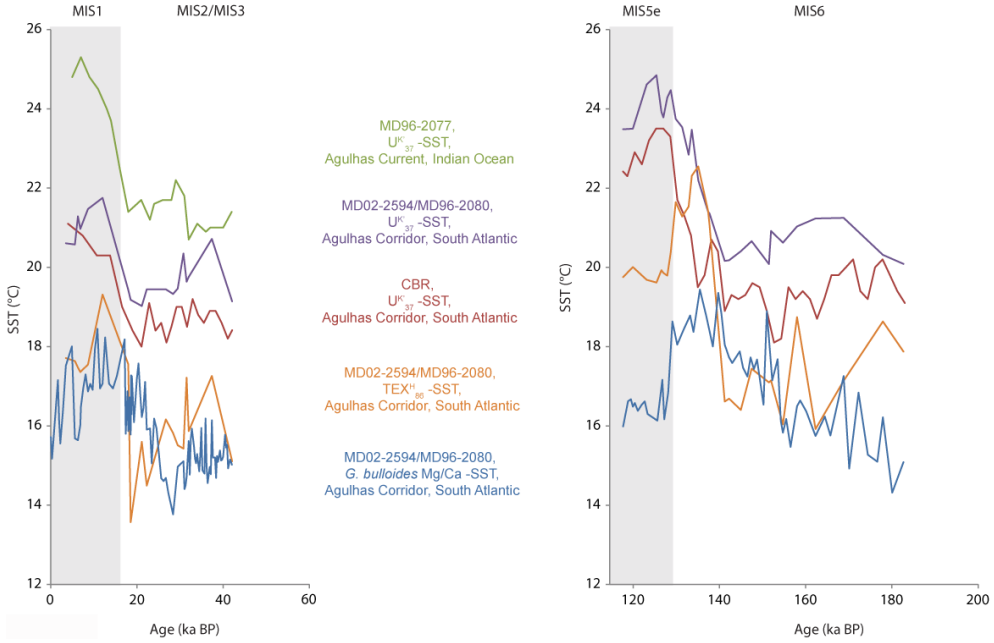

Fig. 4. Comparison of $U^{K'}_{37}$ SST, TEX^{H}_{86} SST and *G. bulloides* Mg/Ca SST (Martinez-Mendez et al., 2010) of **(a)** MIS3-1 (MD02-2594) and **(b)** MIS6-5 (MD96-2080) (see Fig. 1 for core location) with $U^{K'}_{37}$ SST of MD96-2077 in the Agulhas Current, Indian Ocean (Bard and Rickaby, 2009) and $U^{K'}_{37}$ SST of Cape Basin record in the Agulhas corridor, South Atlantic (Peeters et al., 2004).

Table 3. Average values for the hydrogen isotope composition of the $C_{37:2-3}$ alkenones, the global $\delta^{18}O_{ice\ vol.}$ (Waelbroeck et al., 2002), $\delta D_{ice\ vol.}$ (Srivastava et al., 2010) and the local δD_{sw} derived from $\delta^{18}O$ of *G. bulloides* (Martinez-Mendez et al., 2010) for the intervals of before and after Termination I and II.

	Time interval	$\delta D_{alkenone}$(‰)	$\delta^{18}O_{ice\ vol.}$(‰)	$\delta D_{ice\ vol.}$(‰)	δD_{sw}(‰)
Term. I	before (3.5–8.6 ka, $n = 5$)	-188 ± 5	0.06 ± 0.05	0.7 ± 0.4	-0.4 ± 0.9
	after (18–37.4 ka, $n = 11$)	-174 ± 4	0.83 ± 016	6.3 ± 1.2	6.5 ± 2.6
Term. II	before (117.7–129.8 ka, $n = 9$)	-194 ± 3	0.00 ± 0.05	0.3 ± 0.4	-0.5 ± 2.7
	after (141.2–162.3 ka, $n = 8$)	-180 ± 3	0.88 ± 013	6.7 ± 0.9	9.6 ± 2.4

G. oceanica never exceeded the relative abundance of *E. huxleyi*, and it is therefore unlikely that species composition changes had a large impact on $\delta D_{alkenone}$ values during Termination II. During Termination I *E. huxleyi* reached its maximum relative abundances compared to *G. oceanica* (Flores et al., 1999) possibly resulting in more positive $\delta D_{alkenone}$ values rather than the observed trend toward more depleted values (Schouten et al., 2006). Therefore, the observed trends towards more depleted values in the $\delta D_{alkenone}$ during the glacial terminations are most likely not affected significantly by changes in the coccolithophore species composition.

Thus, our observed isotope shifts can likely only be explained by a shift in the δD of water, through global ice volume changes, and/or salinity. We estimate the effect of changes in global ice volume on the $\delta D_{alkenone}$ by using the global mean ocean $\delta^{18}O_{sw}$ record based on benthic Foraminifera (Waelbroeck et al., 2002) and calculated an equivalent δD_{sw} record by applying a local Indian Ocean meteoric waterline (Srivastava et al., 2010). Changes in global δD_{sw} due to the ice volume effect are estimated to be approximately -6 ‰ during both terminations (Table 3). This shift is smaller than that observed in $\delta D_{alkenone}$, suggesting an increase in hydrogen isotopic fractionation during the two terminations.

The residual $\delta D_{alkenone}$ shift likely reflects changes in sea surface salinity. We find alkenones relatively enriched in D during the glacials MIS6 and MIS2/3 and relatively depleted in D during MIS5e and MIS1, suggesting lower salinities during interglacials compared to glacials (Figs. 2, 3). Indeed, reconstructed $\delta^{18}O_{sw}$ from the planktonic Foraminifera *G. bulloides* also indicates higher salinity throughout the glacials MIS6 and MIS3/MIS2 (Figs. 2, 3) (Martinez-Mendez et al., 2010). However, alkenone δD values begin to shift toward more depleted values shortly before

the start of Termination II, at approximately 135 ka, whereas the initial freshening recorded in the $\delta^{18}O_{sw}$ begins at about 133 ka (Fig. 2). Similar diverging trends are noted for reconstructed $\delta^{18}O_{sw}$ derived from the planktonic Foraminifera *G. ruber* (Marino et al., 2013). The most depleted values are reached in both reconstructed $\delta^{18}O_{sw}$ and $\delta D_{alkenone}$ during early MIS5e at about 128 ka (Fig. 2). Higher salinity conditions are also observed throughout MIS3/MIS2 in reconstructed $\delta^{18}O_{sw}$ and $\delta D_{alkenone}$ (Fig. 3) followed by freshening trends starting during early Termination I ($\sim$ 18 ka). The offset in timing of the start of the freshening trends between the different proxies is similar to that observed in the Mg/Ca and $U^{K'}_{37}$ temperature records. This might be explained by differences in depth habitat between haptophyte algae and the Foraminifera and/or salinity effects on Mg/Ca and consequently the reconstructed $\delta^{18}O_{sw}$ record. Despite the discrepancy in the timing of the start of the freshening events, an overall increase in salinity is recorded in both $\delta^{18}O_{sw}$ and $\delta D_{alkenone}$ during glacial stages MIS6 and MIS3/5. This is followed by a rapid decrease in salinity during the terminations. The fresher conditions prevail during the subsequent interglacial stages.

Absolute salinity estimates are difficult to obtain from the $\delta D_{alkenone}$ due to the uncertainties in both the slope and intercept of the culture calibrations and other variables (Rohling, 2007). However, by estimating relative salinity changes only, using the slope of the $\delta D_{alkenone}$–salinity relationship, we avoid uncertainties related to the intercept. This provides an added advantage that the slopes for *E. huxleyi* or *G. oceanica* are nearly identical (i.e., 4.8 ‰ and 4.2 ‰ $\delta D_{alkenone}$ per salinity unit, respectively; Schouten et al., 2006). Estimations for relative salinity changes from $\delta D_{alkenone}$ result in a freshening trend of approximately 1.7–1.9 salinity units during the course of Termination I and II. These results are in fairly good agreement with the estimated salinity shift of 1.2–1.5 based on combined Mg/Ca SST estimates and $\delta^{18}O$ of *G. bulloides* for these time periods (Martinez-Mendez et al., 2010). However, they both seem to differ from the $\delta^{18}O_{sw}$ record based on *G. ruber*, which indicates no salinity difference between glacial–interglacial and only an intermittent shift during the terminations (Marino et al., 2013).

3.3 Paleoceanographic implications

Based on the reconstructed SST and relative SSS records, we suggest that increased salinity during glacial periods and subsequent freshening during the glacial terminations can be explained by the efficiency of the Agulhas leakage (i.e., the volume transport of water from the Indian Ocean to the South Atlantic). According to Peeters et al. (2004), $U^{K'}_{37}$ SST maxima correspond to maximum Agulhas leakage, as seen in the planktonic Foraminifera Agulhas leakage fauna, during glacial Termination I and II. We observe enriched $\delta D_{alkenone}$ values, suggesting increased salinity, coinciding with reduced Agulhas leakage during glacial stages MIS6 and MIS2/3. We suggest that with reduced throughflow and increased residence time of Indian Ocean water, the surface waters become relatively more saline and cooler in the Agulhas region, including the Agulhas leakage area. In contrast, with higher transport rates the surface waters will retain more of the original temperature and salinity resulting in the reconstructed lower salinities and higher temperatures. Thus, temperature and salinity are likely decoupled in this setting. In this case, heat loss is enhanced when water masses flow polewards. Salinity, however, will be retained, and during low through-flow situations in relatively dry glacial periods, evaporation will increase sea surface salinity. At the same time, the limited precipitation and river runoff in this region will not counteract this increase sufficiently. However, the absolute amount of salt that is released into the Atlantic Ocean would still increase during terminations due to the increased flow, even though the surface waters become less saline. Consequently, this would lead to increasing the Atlantic Meridional Overturning Circulation (Bard and Rickaby, 2009; Haarsma et al., 2011).

4 Conclusions

In this study, we analyzed two sediment cores from the Agulhas leakage area covering Termination I and Termination II. We combined TEX^{H}_{86} and $U^{K'}_{37}$ SST reconstructions with a previously reported SST record based on Mg/Ca of the planktonic Foraminifera *G. bulloides* (Martinez-Mendez et al., 2010). Sea surface temperatures reconstructed from three different proxies indicated relatively low temperature conditions throughout the late glacials MIS6 and MIS2/3 in the Agulhas leakage area, and at the onset of the deglaciation (Termination I and II) temperatures increase significantly. Relative salinity changes were reconstructed using $\delta D_{alkenone}$, which showed a shift from more positive values to more negative values during Termination I and Termination II suggesting elevated salinities during glacial periods, with subsequent freshening during glacial terminations. Similar trends in glacial to interglacial salinity changes were also observed based on planktonic Foraminifera $\delta^{18}O_{sw}$ reconstructions. Estimated salinity changes, based on $\delta D_{alkenone}$, range from 1.7 to 1.9 salinity units for Termination I and II. This is in fairly good agreement with salinity shifts based on the paired Mg/Ca and $\delta^{18}O$ approach of the planktonic Foraminifera *G. bulloides*. Our results therefore suggest an increased release of slightly less saline Indian Ocean water to the South Atlantic Ocean during the terminations than during the glacials, but with a net increase in salt transport during interglacials due to the higher throughflow.

Acknowledgements. We acknowledge financial support from the Seventh Framework Programme PEOPLE Work Programme, grant 238512 (Marie Curie Initial Training Network GATEWAYS). The Netherlands Organization for Scientific Research (NWO) is

acknowledged for funding Marcel van der Meer (VIDI) and Stefan Schouten (VICI). S. Kasper would like to thank C. A. Grove (Royal NIOZ, the Netherlands) and D. Chivall (Royal NIOZ, the Netherlands) for their input on this manuscript.

Edited by: G. M. Ganssen

References

Arbuszewski, J., deMenocal, P., Kaplan, A., and Farmer, E. C.: On the fidelity of shell-derived $\delta^{18}O_{sw}$ estimates, Earth Planet Sci. Lett., 300, 185–196, doi:10.1016/j.epsl.2010.10.035, 2010.

Bard, E.: Comparison of alkenone estimates with other paleotemperature proxies, Geochem. Geophys. Geosyst., 2, 1002, doi:10.1029/2000gc000050, 2001.

Bard, E. and Rickaby, R. E. M.: Migration of the subtropical front as a modulator of glacial climate, Nature, 460, 380–U393, doi:10.1038/nature08189, 2009.

Bertrand, P.: Les rapport de campagne a la mer a bord du Marion Dufresne – Campagne NAUSICAA – Images II – MD105 du 20/10/96 au 25/11/96, Inst. Fr. pour la Rech. et la Technol. Polaires, France, Plouzane, 1997.

Biastoch, A., Boning, C. W., and Lutjeharms, J. R. E.: Agulhas leakage dynamics affects decadal variability in Atlantic overturning circulation, Nature, 456, 489–492, 2008.

Bidigare, R. R., Fluegge, A., Freeman, K. H., Hanson, K. L., Hayes, J. M., Hollander, D., Jasper, J. P., King, L. L., Laws, E. A., Milder, J., Millero, F. J., Pancost, R., Popp, B. N., Steinberg, P. A., and Wakeham, S. G.: Consistent fractionation of ^{13}C in nature and in the laboratory: Growth-rate effects in some haptophyte algae, Global Biogeochem. Cy., 11, 279–292, 1997.

Curry, W. B. and Crowley, T. J.: The $\delta^{13}C$ of equatorial Atlantic surface waters: Implications for Ice Age pCO_2 levels, Paleoceanography, 2, 489–517, doi:10.1029/PA002i005p00489, 1987.

D'Andrea, W. J., Liu, Z., Alexandre, M. D. R., Wattley, S., Herbert, T. D., and Huang, Y.: An Efficient Method for Isolating Individual Long-Chain Alkenones for Compound-Specific Hydrogen Isotope Analysis, Anal. Chem., 79, 3430–3435, 2007.

dos Santos, R. A. L., Prange, M., Castaneda, I. S., Schefuss, E., Mulitza, S., Schulz, M., Niedermeyer, E. M., Damste, J. S. S., and Schouten, S.: Glacial-interglacial variability in Atlantic meridional overturning circulation and thermocline adjustments in the tropical North Atlantic, Earth Planet Sci. Lett., 300, 407–414, doi:10.1016/j.epsl.2010.10.030, 2010.

Englebrecht, A. C. and Sachs, J. P.: Determination of sediment provenance at drift sites using hydrogen isotopes and unsaturation ratios in alkenones, Geochim. Cosmochim. Ac., 69, 4253–4265, 2005.

Fallet, U., Ullgren, J. E., Castañeda, I. S., van Aken, H. M., Schouten, S., Ridderinkhof, H., and Brummer, G.-J. A.: Contrasting variability in foraminiferal and organic paleotemperature proxies in sedimenting particles of the Mozambique Channel (SW Indian Ocean), Geochim. Cosmochim. Ac., 75, 5834–5848, doi:10.1016/j.gca.2011.08.009, 2011.

Ferguson, J. E., Henderson, G. M., Kucera, M., and Rickaby, R. E. M.: Systematic change of foraminiferal Mg/Ca ratios across a strong salinity gradient, Earth Planet Sci. Lett., 265, 153–166, doi:10.1016/j.epsl.2007.10.011, 2008.

Flores, J. A., Gersonde, R., and Sierro, F. J.: Pleistocene fluctuations in the Agulhas Current Retroflection based on the calcareous plankton record, Mar. Micropaleontol., 37, 1–22, 1999.

Franzese, A. M., Hemming, S. R., Goldstein, S. L., and Anderson, R. F.: Reduced Agulhas Leakage during the Last Glacial Maximum inferred from an integrated provenance and flux study, Earth Planet Sci. Lett., 250, 72–88, doi:10.1016/j.epsl.2006.07.002, 2006.

Giraudeau, J., Balut, Y., Hall, I. R., Mazaud, A., and Zahn, R.: SWAF-MDI128 Scientific Report, Inst. Polaire Fr., Plouzane, France, 108 pp., 2003.

Haarsma, R. J., Campos, E. J. D., Drijfhout, S., Hazeleger, W., and Severijns, C.: Impacts of interruption of the Agulhas leakage on the tropical Atlantic in coupled ocean-atmosphere simulations, Clim. Dynam., 36, 989–1003, doi:10.1007/s00382-009-0692-7, 2011.

Hönisch, B., Allen, K. A., Lea, D. W., Spero, H. J., Eggins, S. M., Arbuszewski, J., deMenocal, P., Rosenthal, Y., Russell, A. D., and Elderfield, H.: The influence of salinity on Mg/Ca in planktic foraminifers – Evidence from cultures, core-top sediments and complementary $\delta^{18}O$, Geochim. Cosmochim. Ac., 121, 196–213, doi:10.1016/j.gca.2013.07.028, 2013.

Huguet, C., Martrat, B., Grimalt, J. O., Damste, J. S. S., and Schouten, S.: Coherent millennial-scale patterns in $U^{K'}_{37}$ and TEX^{H}_{86} temperature records during the penultimate interglacial-to-glacial cycle in the western Mediterranean, Paleoceanography, 26, Pa2218, doi:10.1029/2010pa002048, 2011.

Karner, M. B., DeLong, E. F., and Karl, D. M.: Archaeal dominance in the mesopelagic zone of the Pacific Ocean, Nature, 409, 507–510, 2001.

Kim, J. H., van der Meer, J., Schouten, S., Helmke, P., Willmott, V., Sangiorgi, F., Koc, N., Hopmans, E. C., and Damste, J. S. S.: New indices and calibrations derived from the distribution of crenarchaeal isoprenoid tetraether lipids: Implications for past sea surface temperature reconstructions, Geochim. Cosmochim. Ac., 74, 4639–4654, doi:10.1016/j.gca.2010.05.027, 2010.

Lee, K. E., Kim, J.-H., Wilke, I., Helmke, P., and Schouten, S.: A study of the alkenone, TEX_{86}, and planktonic foraminifera in the Benguela Upwelling System: Implications for past sea surface temperature estimates, Geochem. Geophys. Geosyst., 9, Q10019, doi:10.1029/2008gc002056, 2008.

Lutjeharms, J. R. E.: The Agulhas Current, Springer, Berlin, 329 pp., 2006.

Marino, G., Zahn, R., Ziegler, M., Purcell, C., Knorr, G., Hall, I. R., Ziveri, P., and Elderfield, H.: Agulhas salt-leakage oscillations during abrupt climate changes of the Late Pleistocene, Paleoceanography, 28, 599–606, doi:10.1002/palo.20038, 2013.

Martinez-Mendez, G., Zahn, R., Hall, I. R., Pena, L. D., and Cacho, I.: 345,000-year-long multi-proxy records off South Africa document variable contributions of Northern versus Southern Component Water to the Deep South Atlantic, Earth Planet Sci. Lett., 267, 309–321, 2008.

Martinez-Mendez, G., Zahn, R., Hall, I. R., Peeters, F. J. C., Pena, L. D., Cacho, I., and Negre, C.: Contrasting multiproxy reconstructions of surface ocean hydrography in the Agulhas Corridor and implications for the Agulhas Leakage during the last 345,000 years, Paleoceanography, 25, 12, Pa4227, doi:10.1029/2009pa001879, 2010.

Müller, P. J., Kirst, G., Ruhland, G., von Storch, I., and Rosell-Melé, A.: Calibration of the alkenone paleotemperature index $U^{K'}_{37}$ based on core-tops from the eastern South Atlantic and the global ocean (60° N–60° S), Geochim. Cosmochim. Ac., 62, 1757–1772, 1998.

Pahnke, K., Sachs, J. P., Keigwin, L., Timmermann, A., and Xie, S.-P.: Eastern tropical Pacific hydrologic changes during the past 27,000 years from D/H ratios in alkenones, Paleoceanography, 22, PA4214, doi:10.1029/2007pa001468, 2007.

Peeters, F. J. C., Acheson, R., Brummer, G. J. A., de Ruijter, W. P. M., Schneider, R. R., Ganssen, G. M., Ufkes, E., and Kroon, D.: Vigorous exchange between the Indian and Atlantic oceans at the end of the past five glacial periods, Nature, 430, 661–665, doi:10.1038/nature02785, 2004.

Penven, P., Lutjeharms, J. R. E., and Florenchie, P.: Madagascar: A pacemaker for the Agulhas Current system?, Geophys. Res. Lett., 33, L17609, doi:10.1029/2006gl026854, 2006.

Prahl, F. G. and Wakeham, S. G.: Calibration of Unsaturation Patterns in Long-Chain Ketone Compositions for Paleotemperature Assessment, Nature, 330, 367–369, 1987.

Rau, A. J., Rogers, J., Lutjeharms, J. R. E., Giraudeau, J., Lee-Thorp, J. A., Chen, M. T., and Waelbroeck, C.: A 450-kyr record of hydrological conditions on the western Agulhas Bank Slope, south of Africa, Mar. Geol., 180, 183–201, 2002.

Rau, G. H., Riebesell, U., and WolfGladrow, D.: A model of photosynthetic ^{13}C fractionation by marine phytoplankton based on diffusive molecular CO_2 uptake, Mar. Ecol. Progr. Series, 133, 275–285, doi:10.3354/meps133275, 1996.

Rohling, E. J.: Paleosalinity: confidence limits and future applications, Mar. Geol., 163, 1–11, 2000.

Rohling, E. J.: Progress in paleosalinity: Overview and presentation of a new approach, Paleoceanography, 22, PA3215, doi:10.1029/2007pa001437, 2007.

Rohling, E. J. and Bigg, G. R.: Paleosalinity and $\delta^{18}O$: A critical assessment, J. Geophys. Res.-Oceans, 103, 1307–1318, 1998.

Rontani, J.-F., Prahl, F. G., and Volkman, J. K.: Re-examination of the double bond positions in alkenones and derivatives: biosynthetic implications, J. Phycol., 42, 800–813, doi:10.1111/j.1529-8817.2006.00251.x, 2006.

Rouault, M., Penven, P., and Pohl, B.: Warming in the Agulhas Current system since the 1980's, Geophys. Res. Lett., 36, L12602, doi:10.1029/2009gl037987, 2009.

Saher, M. H., Rostek, F., Jung, S. J. A., Bard, E., Schneider, R. R., Greaves, M., Ganssen, G. M., Elderfield, H., and Kroon, D.: Western Arabian Sea SST during the penultimate interglacial: A comparison of $U^{K'}_{37}$ and Mg/Ca paleothermometry, Paleoceanography, 24, PA2212, doi:10.1029/2007pa001557, 2009.

Schneider, R. R., Muller, P. J., and Ruhland, G.: Late Quaternary surface circulation in the east equatorial South Atlantic: Evidence from Alkenone sea surface temperatures, Paleoceanography, 10, 197–219, 1995.

Schouten, S., Hopmans, E. C., Schefuß, E., and Sinninghe Damsté, J. S.: Distributional variations in marine crenarchaeotal membrane lipids: a new tool for reconstructing ancient sea water temperatures?, Earth Planet Sci. Lett., 204, 265–274, 2002.

Schouten, S., Ossebaar, J., Schreiber, K., Kienhuis, M. V. M., Langer, G., Benthien, A., and Bijma, J.: The effect of temperature, salinity and growth rate on the stable hydrogen isotopic composition of long chain alkenones produced by Emiliania huxleyi and Gephyrocapsa oceanica, Biogeosciences, 3, 113–119, doi:10.5194/bg-3-113-2006, 2006.

Schouten, S., Huguet, C., Hopmans, E. C., Kienhuis, M. V. M., and Sinninghe Damsté, J. S.: Analytical Methodology for TEX_{86} Paleothermometry by High-Performance Liquid Chromatography/Atmospheric Pressure Chemical Ionization-Mass Spectrometry, Anal. Chem., 79, 2940–2944, doi:10.1021/ac062339v, 2007.

Schwab, V. F. and Sachs, J. P.: The measurement of D / H ratio in alkenones and their isotopic heterogeneity, Org. Geochem., 40, 111–118, 2009.

Srivastava, R., Ramesh, R., Jani, R. A., Anilkumar, N., and Sudhakar, M.: Stable oxygen, hydrogen isotope ratios and salinity variations of the surface Southern Indian Ocean waters, Curr. Sci. India, 99, 1395–1399, 2010.

van der Meer, M. T. J., Baas, M., Rijpstra, W. I. C., Marino, G., Rohling, E. J., Sinninghe Damsté, J. S., and Schouten, S.: Hydrogen isotopic compositions of long-chain alkenones record freshwater flooding of the Eastern Mediterranean at the onset of sapropel deposition, Earth Planet Sci. Lett., 262, 594–600, 2007.

van der Meer, M. T. J., Sangiorgi, F., Baas, M., Brinkhuis, H., Sinninghe Damsté, J. S., and Schouten, S.: Molecular isotopic and dinoflagellate evidence for Late Holocene freshening of the Black Sea, Earth Planet Sci. Lett., 267, 426–434, 2008.

van der Meer, M. T. J., Benthien, A., Bijma, J., Schouten, S., and Sinninghe Damsté, J. S.: Alkenone distribution impacts the hydrogen isotopic composition of the $C_{37:2}$ and $C_{37:3}$ alkan-2-ones in Emiliania huxleyi, Geochim. Cosmochim. Ac., 111, 162–166, doi:10.1016/j.gca.2012.10.041, 2013.

van Sebille, E., Biastoch, A., van Leeuwen, P. J., and de Ruijter, W. P. M.: A weaker Agulhas Current leads to more Agulhas leakage, Geophys. Res. Lett., 36, L03601, doi:10.1029/2008gl036614, 2009.

van Sebille, E., Beal, L. M., and Johns, W. E.: Advective Time Scales of Agulhas Leakage to the North Atlantic in Surface Drifter Observations and the 3D OFES Model, J. Phys. Oceanogr., 41, 1026–1034, doi:10.1175/2010jpo4602.1, 2011.

Waelbroeck, C., Labeyrie, L., Michel, E., Duplessy, J. C., McManus, J. F., Lambeck, K., Balbon, E., and Labracherie, M.: Sea-level and deep water temperature changes derived from benthic foraminifera isotopic records, Quaternary Sci. Rev., 21, 295–305, 2002.

Wuchter, C., Schouten, S., Wakeham, S. G., and Sinninghe Damsté, J. S.: Archaeal tetraether membrane lipid fluxes in the northeastern Pacific and the Arabian Sea: Implications for TEX_{86} paleothermometry, Paleoceanography, 21, PA4208, doi:10.1029/2006pa001279, 2006.